AFRL-OSR-VA-TR-2013-0592

COMPUTATIONAL DYNAMICS OF METAL-CARBON INTERFACE--
KEY TO CONTROLLABLE NANOTUBE GROWTH

BORIS YAKOBSON

WILLIAM MARSH RICE UNIVERSITY

11/13/2013
Final Report

AIR FORCE RESEARCH LABORATORY
AF OFFICE OF SCIENTIFIC RESEARCH (AFOSR)/RSA
ARLINGTON, VIRGINIA 22203
AIR FORCE MATERIEL COMMAND

REPORT DOCUMENTATION PAGE

1. REPORT DATE *(DD-MM-YYYY)*	2. REPORT TYPE	3. DATES COVERED *(From - To)*
9-11-2013	final report	rom 1 July 2012 to 30 June 2013

4. TITLE AND SUBTITLE	5a. CONTRACT NUMBER
Computational Dynamics of Metal-Carbon Interface — Key to Controllable Nanotube Growth	FA9550-10-1-0287

5b. GRANT NUMBER
FA9550-10-1-0287

5c. PROGRAM ELEMENT NUMBER

6. AUTHOR(S)	5d. PROJECT NUMBER
Boris I. Yakobson	

5e. TASK NUMBER

5f. WORK UNIT NUMBER

7. PERFORMING ORGANIZATION NAME(S) AND ADDRESS(ES)	8. PERFORMING ORGANIZATION REPORT NUMBER
Rice University 6100 Main Street, MS 321 Houston, TX 77005	

9. SPONSORING / MONITORING AGENCY NAME(S) AND ADDRESS(ES)	10. SPONSOR/MONITOR'S ACRONYM(S)
AFOSR 875 North Randolph Street Arlington, VA 22203	AFOSR

11. SPONSOR/MONITOR'S REPORT NUMBER(S)

12. DISTRIBUTION / AVAILABILITY STATEMENT

Distribution A - Approved for public release

13. SUPPLEMENTARY NOTES

14. ABSTRACT

During this final year of the project we have completed an extensive analysis of the energy landscape for the nanotube caps to elucidate its role in the chiral distribution at the nucleation stage of nanotube growth, as described in a submitted paper. Massive computations performed on about 5000 topologically distinguishable caps with precise classical potential (additionally validated on a subset of ~100 cap computed with density functional theory methods) show relatively flat landscape, which should not affect chiral selectivity. Further, we completed the "first release" of our quantitative nanoreactor diagram (or model). Through detailed description of the catalyst-carbon interface, defects energies, and growth rate, this approach makes predictions of nanotube distribution or graphene sheet shape, verifiable experimentally. Important findings in experimental growth provide strong support to the step-flow approach augmented by DFT computations. This allowed us to readily calculate the rate of nanotube or graphene growth, on different catalyst metals such as Fe, Ni, Co, Cu. We also completed our study of cooperative behavior in growth of nanotube forests, their simulated kinetics with the account for the lateral forces and feedback mechanism.

15. SUBJECT TERMS

carbon, nanotubes, chiral symmetry, nucleation, caps, topology

16. SECURITY CLASSIFICATION OF:			17. LIMITATION OF ABSTRACT	18. NUMBER OF PAGES	19a. NAME OF RESPONSIBLE PERSON Boris I. Yakobson
a. REPORT	b. ABSTRACT	c. THIS PAGE	UU	21	19b. TELEPHONE NUMBER *(include area code)*
UU	UU	UU			713-348-3572

FINAL PROGRESS REPORT

Contract/Grant Title: "Computational Dynamics of Metal-Carbon Interface — Key to Controllable Nanotube Growth"
Contract/Grant #: FA9550-10-1-0287
Final Reporting Period: 1 July 2012 to 30 June 2013
Full Project Period 1 July 2010 to 30 June 2013

Following the Abstract, below we detail our developments, giving particular attention and detail to yet unpublished results, while only briefly mentioning material which is already fully available in publications.

I. Energy landscape of carbon nanotube caps: lack of intrinsic chirality bias and consequences for selective growth

Treating the chance for a carbon nanotube (CNT) of a chiral angle χ to emerge from the "primordial soup" of carbon atoms on the catalyst as determined by their relative energies, here we present large-scale calculations designed to evaluate the "elastic" energies of all possible CNT caps (obeying the isolated pentagon rule) for selected chiralities (n,m) corresponding to tube diameters $d \leq 1$ nm. Our quantitative analysis shows that the energy scale associated with the CNT caps is small, compared to that of the CNT/catalyst interface. Such a flat energy landscape is irrelevant to chiral selectivity and lends further credibility to interface-controlled scenarios for selective growth of single-walled CNTs.

Carbon nanotubes (CNTs) have revitalized fundamental and applied nanosciences in an unprecedented fashion. Even two decades after the seminal works[1] in the field, deep understanding of their growth mechanism is still elusive.[2] Depending on their type (n,m), nanotubes can have semiconducting or metallic electronic properties, and selectively growing nanotubes of the desired types is therefore a crucial scientific goal. Alternatively to the chiral indices n and m, the nanotube type can be described by the combination of nanotube diameter $d = \frac{a}{\pi}(n^2+m^2+nm)^{1/2}$, a being the lattice constant, and chiral angle $\chi = \arctan(\sqrt{3}m/(m+2n))$ which determines the direction of rolling-up of the graphene lattice,[3] to form the nanotube. Since it is usually easier to control the diameter during growth (e.g., by adjusting the catalyst nanoparticle size) or to purify nanotubes by diameter after synthesis, the problem of selective CNT growth is often phrased in terms of the sub-goal of controlling the chiral angle χ. Further, because it is hard to change nanotube type after growth has reached the repetitive stage, a natural focus is the nucleation stage: this is where both the diameter and chiral angle are believed to be set in.

In the pursuit of routes towards chiral selectivity,[4] the importance of the nucleation stage in the CNT growth has long been recognized and extensively studied both experimentally and theoretically for various growth scenarios.[5-15] Within the classical nucleation theory, the change in the Gibbs free energy upon formation of a sp^2 nucleus of N atoms is composed of a "bulk" term $\sim N$ and an edge term[15] $\sim N^{1/2}$. This energy decomposition has been well explored for the archetypal system of a graphene island on a metal substrate[16-19] as well as in the case of phase separation in graphene functionalization.[20, 21] On a finite-size particle, e.g., of radius R, the carbon nucleus has to accommodate mean curvature $\sim 1/R$ by incorporating pentagonal "defects"—disclinations—which leads to an elastic energy penalty[22-25] $\sim \ln N$.

Since the CNT diameter d is constrained by the catalyst nanoparticle size,[26-28] typically it is assumed that the energy of the nanotube cap (comprising six pentagons) emerging from the initial nucleus is essentially independent of the CNT chirality χ. This simple argument allows one to focus exclusively on essential χ-

dependent contributions to the total energy of the CNT–catalyst system, Figure 1 inset. Recently, Liu *et al.*[29] have analyzed the energetics of the CNT–catalyst interface based on atomistic calculations of the "edge" energy dependence on χ using graphene edge as a model. However, the attempts so far to quantify E^{cap} are scarce and limited to just a handful of caps and chiral indices (n,m),[30-32] although various aspects of the caps structure and energetics have been addressed in a number of studies.[7, 17, 33-37] The 1999 census of CNT caps,[38] however, has revealed a rather crowded caps population where, empirically, the number of nanotube caps $N^{cap}(d) \sim d^{v}$, with $v \approx 8$.[31, 38] This large exponent implies an enormous N^{cap} even for caps with isolated pentagons, leaving the effect of configurational diversity on CNT–cap energetics practically unexplored, with the exception of perhaps a single study[31] of the (10,0) zigzag tube with $N_{10,0}{}^{cap} = 7$.[38] Since any multiplicity of caps results in a configurational entropy contribution $k_B \ln N_{n,m}{}^{cap}$, with k_B the Boltzmann constant, the strong diameter dependence of the cap numbers has been invoked early on to rationalize the experimentally observed preference for larger-diameter tubes.[39, 40]

Such a configurational variety may (informally) be looked at from a materials informatics perspective. A fixed pattern of six pentagons "encodes" what unique (n,m) chirality a nascent nanotube would inherit. In this sense it can be viewed as the "inorganic gene"[41, 42] of a CNT. Although the chirality code is written in a single "letter" (a pentagon, unlike the four-letter DNA alphabet, for instance), its effective two-dimensionality (set by the sp^2 C hybridization) allows for multiple six-pentagon configurations that can be aptly "sequenced" in the language of graph theory.[38] The present effort thus aims to establish a quantitative structure–property (intrinsic elastic energy) relation for a set of more than 4500 caps corresponding to 21 chiralities. This is achieved by a systematic study of CNT cap energetics over the *whole range* of chiral angles $0° \leq \chi \leq 30°$ based on large-scale atomistic calculations of *all* possible caps with isolated pentagons for selected values of d.
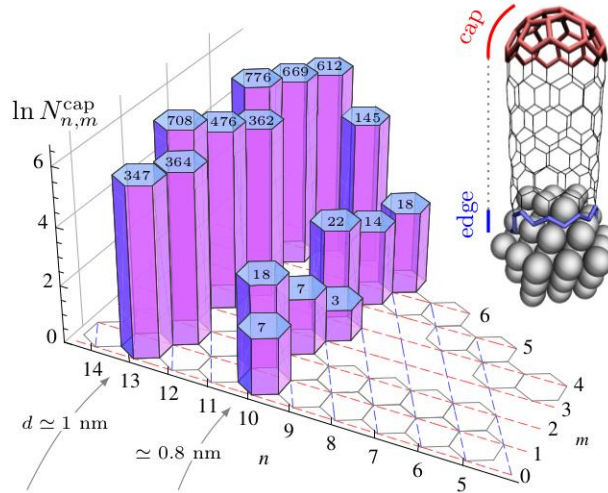

Figure 1: Logarithm of the number of all possible nanotube caps $N_{n,m}{}^{cap}$ with isolated pentagons for the (n,m) pairs considered in the present work (actual cap numbers are shown atop the corresponding prismatic bars). Inset: Schematic representation of (energy) partitioning for a CNT formed on a catalytic nanoparticle, with the CNT cap and edge highlighted.

Results and Discussion

Here we consider two sets of nanotubes, whose chiral angles sweep the full zigzag-to-armchair range, and correspond to two diameter constraints: $d \approx 0.8$ nm ($N^{cap} = 89$) and $d \approx 1$ nm ($N^{cap} = 4459$), respectively. Figure 1 shows N^{cap} for the selected (n,m) pairs. More details are given in the Methods section. Note that, as χ varies, a d = const condition cannot be strictly fulfilled and diameters differ by ~ 5%. In choosing the

set of chiral indices, we have mandated that there exist at least two caps that would fit given (n,m) tube, $N_{n,m}^{cap} > 1$, leading to a smaller-d set of chiralities, with $d \approx 0.8$ nm. The set representing $d \approx 1$ nm, has much larger N^{cap}, yet feasible computationally. It is also the minimal diameter beyond which the number of caps appears to approach the $\sim d^8$ asymptotic dependence.[31]
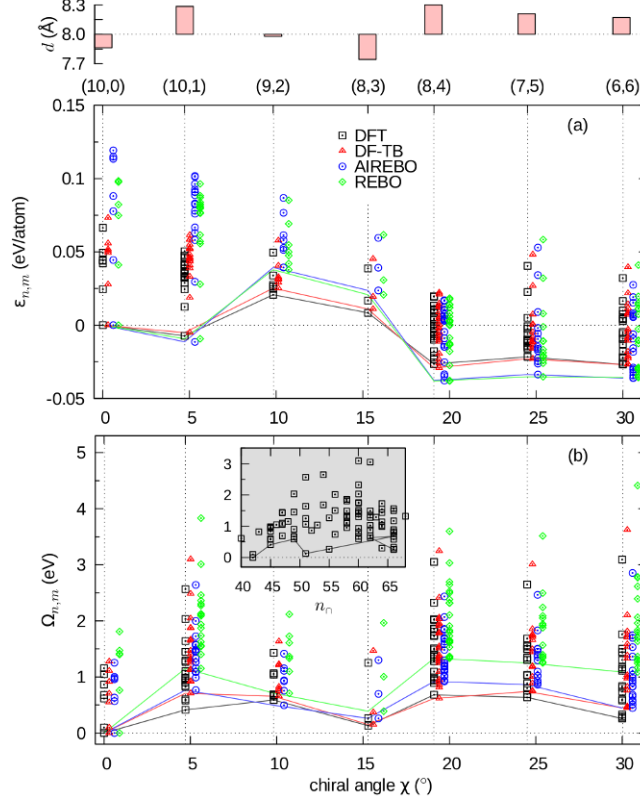

Figure 2: (a) Cap energy $\varepsilon_{n,m}$, according to eq. 1, for $d \approx 0.8$ nm relative to $\varepsilon_{10,0} \equiv \varepsilon_{\chi=0}$. Lines connect the minimal energies, $\min_i \varepsilon^{(i)}_{\chi=const}$, for given computational method. For clarity, calculated points are slightly offset for each method. The actual CNT diameters d are given in the top panel (bars, relative to a reference value $d_0 = 0.8$ nm); (b) Similar to (a), but for $\Omega_{n,m}$, according to eq. 3. The inset shows the DFT-calculated $\Omega_{n,m}$ vs the number of C atoms in the cap $n_\cap$.

Here we explore the ground-state energy landscape in terms of the CNT cap energy defined as

$$\varepsilon_{n,m} = \varepsilon'_{n,m} - \mu_g$$
$$\equiv \frac{1}{n_\cap} [E_{n,m}^{tot}(N) - (N-n_\cap)\mu_{n,m}^{CNT}] - \mu_g, \qquad (1)$$

where $E_{n,m}^{tot}(N)$ is the total potential energy of the system of N carbon atoms representing the capped CNT for given (n,m), $\mu_{n,m}^{CNT}$ is the cohesive energy per atom in an ideal infinite CNT of the same chirality, μ_g is that for graphene and $n_\cap$ is the number of atoms in the cap. As defined in eq. 1, the cap energy is a *per atom* excess quantity with graphene as a reference. The actual value of $n_\cap$ is linked to the particular cap enumeration algorithm and thereby subject to the provisions made in Refs.[38, 43] regarding the choice of a boundary between the CNT and the cap. An immediate implication is that such a boundary, as pointed out by Brinkmann *et al.*,[38, 43] e.g., for a capped (n,n) tube may not be strictly of armchair type (see Figure 4 below). By construction, however, for given (n,m) the algorithm guarantees that the caps have identical embedding $(N-n_\cap)$, or "layers" of hexagons, as described in the Methods section.

3

One can further rewrite eq. 1 in an equivalent form

$$\varepsilon_{n,m} = \Omega_{n,m}/n_\cap + \mu_{n,m}^{CNT} - \mu_g \qquad (2)$$

to separate the CNT elastic bending energy[24, 44-48] $\mu_{n,m}^{CNT} - \mu_g \sim 1/d^2$ inherent to the definition eq. 1. The grand-potential term

$$\Omega_{n,m} \equiv E_{n,m}^{tot}(N) - N\mu_{n,m}^{CNT} \qquad (3)$$

is then the *total* energy cost of transforming a (*n*,*m*) CNT into a capped tube with the same number of atoms *N* and chirality and is invariant with respect to the CNT–cap boundary choice.
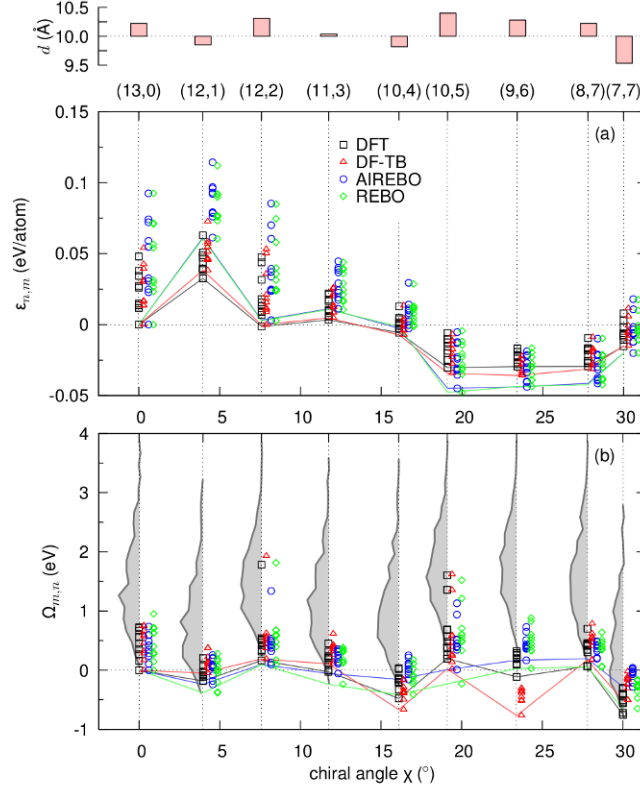
Figure 3: Similar to Figure 2, but for the set of caps with $d \approx 1$ nm, relative to $\varepsilon_{13,0} \equiv \varepsilon_{\chi=0}$. The gray filled lines in (b) represent the energy histograms of *all* 4459 caps, calculated with DF-TB, using 0.2 eV bins.

Such definitions are indeed expedient in the context of the poorly defined boundary between the cap and the CNT, as already mentioned above. Without the $\mu_{n,m}^{CNT}$ term, "moving" the cap-CNT boundary, $n_\cap \rightarrow n_\cap \pm \Delta n_\cap$ (for example, excluding/adding a carbon dimer from/to a locally armchair section of the initial boundary), would result in a bias $\Delta n_\cap(\mu_{n,m}^{CNT} - \mu_g)$.

(10,0) (10,1) (9,2) (8,3) (8,4) (7,5) (6,6)

$\bar{L}$	2.8	3.13	3.0	2.73	3.13	3.2	3.0
L_{max}	6	7	7	5	7	7	6

$\bar{L}$	4.53	4.27	4.6	4.33	4.07	4.33	4.33	4.33	3.87
L_{max}	8	8	9	7	7	7	8	8	7

(13,0) (12,1) (12,2) (11,3) (10,4) (10,5) (9,6) (8,7) (7,7)

0

5

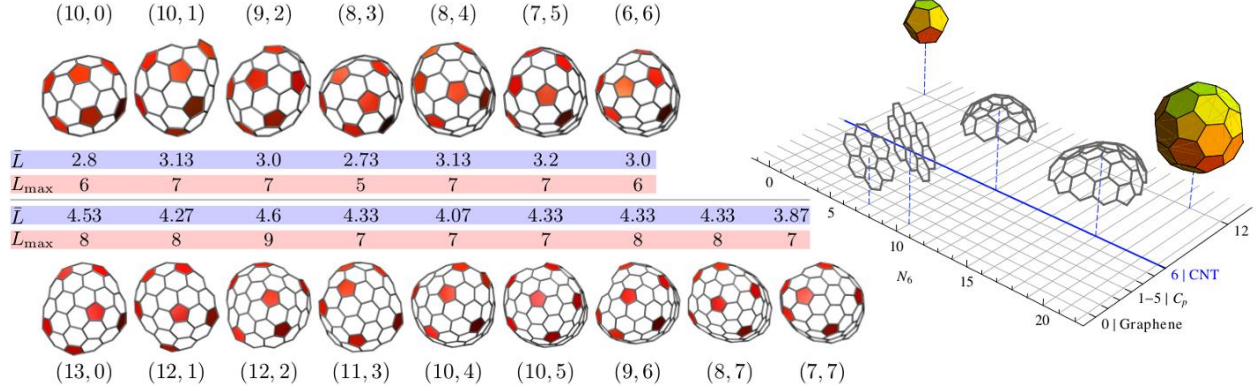10

N_6 15

20

12

6 | CNT

1–5 | C_p

0 | Graphene

Figure 4: Cap geometries with the lowest $\Omega_{n,m}$ values calculated with DFT. All pentagonal rings are highlighted.[49, 50] The largest element L_{max} and the mean of all elements $\overline{L}$ of the corresponding distance matrices, eq. 5, are given as well. Inset: Schematic map of some cyclic carbon structures in the (N_6,N_5)-plane. The C_p lines correspond to cone structures[29] with p pentagons. All caps/CNT considered can be mapped onto the $N_5 = 6$ highlighted line. A few examples are explicitly rendered: the C_{20} dodecahedron at (0,12), the C_{60} buckyball at (20,12), the (10,0)-cap at (11,6) and (13,0)-cap at (18,6), coronine at (7,0) and ovalene at (10,0).

All cap energies calculated from eq. 1 for $d \approx 0.8$ nm using two reactive bond-order empirical potentials (REBO and AIREBO) and two quantum-mechanical methods, density-functional theory (DFT) and DFT-based tight binding (DF-TB) (see the Methods section for computational details) are plotted in Figure 2a. The minimal $\varepsilon_{n,m}$, regardless of the computational method, lie in an energy window of ≈ 0.1 eV/atom, which for typical growth conditions is $\sim k_B T$, T being the temperature, with caps towards the armchair end displaying slightly lower $\varepsilon_{n,m}$ values. It is evident that the configurational minimization

$$\min_i \varepsilon^{(i)}_{\chi =\text{const}}, \qquad\qquad 1 \le i \le N_{n,m}{}^{\text{cap}} \qquad\qquad (4)$$

(i being the cap index for given (n,m), see also Figure 1), is crucial in assessing the relative stability as the actual pentagonal pattern can bring about energy variation of up to ≈ 0.1 eV, especially when evaluation employs the empirical potentials.

The graph reveals clearly the scale of variation in the cap energies over the whole range of chiral angles. The configurationally minimal energies $\min_i \varepsilon^{(i)}$, Figure 2a, are those corresponding to the caps with largest $n_\cap$ for given (n,m); note that for some chiralities there exist a whole subset of $N_{n,m}{}^{\text{cap}}$ of caps (i.e., more than one) with largest $n_\cap$. Ranking of higher-energy structures is however not monotonous with respect to $n_\cap$. The min $\varepsilon_{n,m}$ variation with the chiral angle χ is very similar for all computational schemes employed; the DFT-based methods and the empirical potentials form two pairs, practically indistinguishable within the computational accuracy. It should be noted that within DFT and DF-TB fully agree in identifying the same cap isomers are lowest-energy configurations for practically all (n,m). Similarities between the methods are apparent also in the $\Omega_{n,m}$ plots, Figure 2b. As total quantities, $\Omega_{n,m}$ vary over a wider energy scale, ~ 0.5–1 eV, and qualitatively follow the trend in the CNT diameters d, whose actual values are given in the top panel of Figure 2. However, there is no clear correlation between the minimal-$\Omega_{n,m}$ envelope of all configuration and the size of the caps $n_\cap$, Figure 2b inset.

The energetics of the larger CNT caps for $d \sim 1.0$ nm requires computation of $E_{n,m}{}^{\text{tot}}$ of a huge number of structures, Figure 1, which is a daunting task especially at the DFT level. Exploiting the very good agreement between DFT and DF–TB for the smaller set, Figure 2, selection of structures to be calculated and compared with all the four methods was based on the DF-TB-calculated energies of all $N^{\text{cap}} = 4548$

5

configurations as explained in the Methods section. The energies of the reduced set of 90 structures for d ~ 1.0 nm, calculated from eq. [1] and eq. [3], are plotted in Figure [3]. We shall note that practically the whole discussion above regarding the energetics in Figure [2] is applicable also to the case of larger-diameter capped tubes, Figure [3]. A representative example of all energies calculated with the DF-TB method is given in Figure [3]b; because of the large number of structures we show the energy histograms that can be viewed as "density of cap states". Note that the configurational diversity accounts for ≈ 4 eV spread in $\Omega_{n,m}$. The lowest-$\Omega_{n,m}$ geometries of all 16 chiralities from Figure [2] and Figure [3] as obtained from DFT are rendered in Figure [4]. As all caps incorporate exactly $N_5 = 6$ pentagons, there is one-to-one correspondence between $n_\cap$ and the number of hexagons N_6 in the cap. Thus, in the (N_5, N_6) plane, these structures are mapped onto a set of discrete points lying along the $N_5 = 6$ line as sketched in the inset of Figure [4].

It is well understood that among the possible configurations of six pentagons, those that obey the isolated-pentagon rule (as all geometries considered here do) are most favorable energetically.[31, 51] Rationalizing the energy ranking within the sets of $N_{n,m}^{cap}$ structures for each (n,m) is no longer straightforward as alluded to in the studies on the isolated-pentagon fullerenes.[51] We have explored possible correlations between $\Omega_{n,m}$ and some basic characteristics of the corresponding cap graphs.[38, 51] Specifically, we consider the pentagon-pentagon distance matrix L with elements

$$L_{pq} = (1-\delta_{pq})l_{pq}, \qquad (5)$$

where δ_{pq} is the Kronecker delta and l_{pq} is the shortest path in terms of number of bonds that connects an atom from pth pentagon with an atom from qth pentagon. Note that the isolated-pentagon rule is simply equivalent to $\min_{p,q} L_{pq} \geq 1$. In Figure [4] we report the largest element (longest distance) L_{max} and the mean of all matrix elements $\overline{L}$ for the corresponding lowest-$\Omega_{n,m}$ geometries. We do not find, however, any systematic correlation between the energy ranking and the distance-based invariants of the cap graph,[51] e.g., hexagon neighbor index or those related to the spectrum of L.
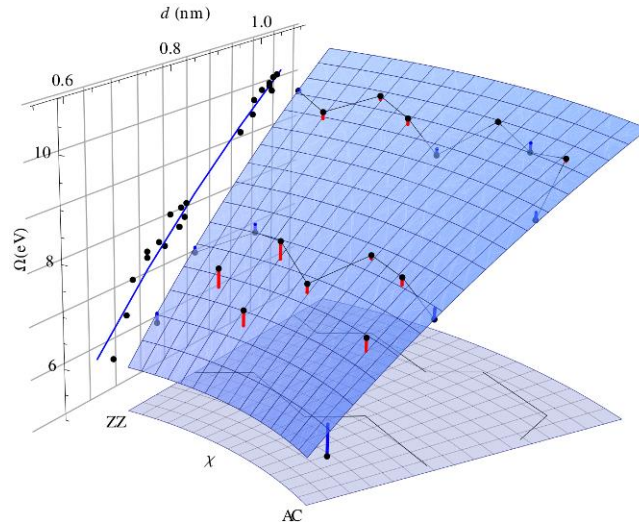
Figure 5: Polar plot of the $\Omega_{n,m}$ surface obtained by revolving the $\Omega_{n,m}(d)$ fit (blue curve on the (d,Ω)-face of the graph) to the calculated DFT points over the chiral angle $0° \leq \chi \leq 30°$. The two DFT data sets from Figure [2] and Figure [3] are extended with five trivial cases for which $N_{n,m}^{cap} \equiv 1$: (9,0), (9,1), (8,2), (6,5), and (5,5). The distance of the calculated points to the analytical surface is indicated by impulses (above: red; below: blue).

The merit of quantifying the CNT cap energetics is best revealed when considering $\Omega_{n,m}$ in the two-dimensional parameter space (d,χ). It is straightforward to further extend the set of structures, Figure 1, with five trivial cases of (n,m) tubes, each having just a single isolated-pentagon cap: the achiral (9,0) and (5,5) with $d \approx 0.7$ nm, and the chiral (9,1), (8,2) and (6,5) tubes. The resulting extended set of points, calculated using DFT, is shown in Figure 5. In a zero-order approximation, the excess energy attributed to the CNT cap is considered as an essentially elastic curvature energy and thereby χ-independent,

$$\Omega_{n,m} \sim \ln d. \qquad (6)$$

Indeed, approximating the cap as a superposition of six "cones", one can write its elastic energy E in the form[22, 24, 25]

$$E = E_{core} + \frac{11}{5} \pi D \ln(\overline{r_{max}}/a), \qquad (7)$$

where E_{core} is the local contribution from the pentagon disclinations, D the bending rigidity of graphene, $\overline{r_{max}} = (\Pi_p^6 r_{max,p})^{1/6}$ the geometric mean of the "lengths" of the six cones, and a is a cutoff of the order of the bond length. For the pth pentagon, $r_{max,p}$ may be chosen as half of the nearest-pentagon-neighbor distance, i.e., $2r_{max,p}/a \sim \min_q L_{pq}$. The $\ln d$-fit to the calculated points is given on the (d,Ω)-face of the plot in Figure 5 and results in $D \approx 1.3$ eV in excellent agreement with the values $D \approx 1.1$–1.5 eV reported in previous works using the same computational methods.[22, 48, 52] Within such a picture, the variation in the minimal caps energies from Figure 2b and Figure 3b appears to reflect the differences in the discrete tube diameter d (cf. the projected lines onto the base-plane of Figure 5). One can formally obtain a $\Omega(d,\chi)$ surface by revolving $\Omega(d)$ over the chiral angle $0° \leq \chi \leq 30°$, as shown in Figure 5.
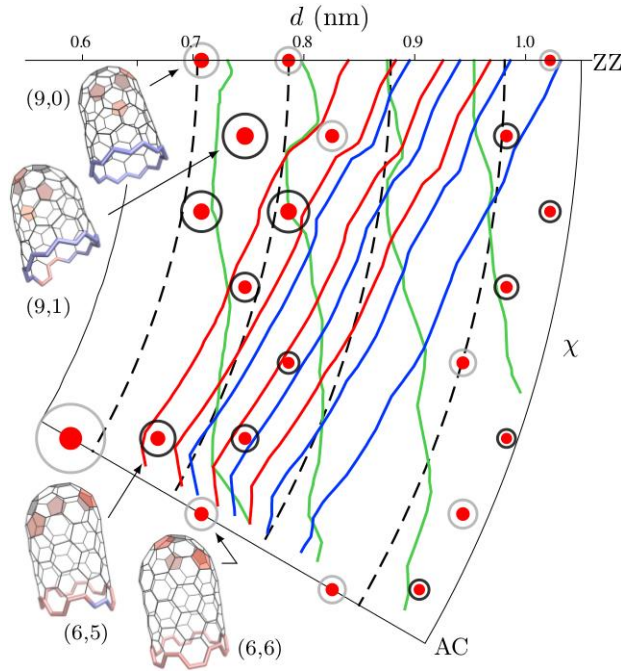
Figure 6: Polar plot of the $\Omega + \Gamma$ surface in the (d,χ) plane. The dashed contours correspond to the analytical Ω surface in Figure 5 and the open circles size corresponds to the impulses length in Figure 5. For clarity, only energy slices of 3 eV width are rendered and isoenergy contour-line spacing is 1 eV in all cases. $\gamma_{AC,ZZ}$ edge energies, cf. eq. 8, for hydrogen termination (green), using H_2 reservoir, are taken from Ref.[29] and for Fe (red) and Co (blue) from Ref.[53]. Images illustrate a few geometries with both the pentagon pattern and edge highlighted.

The lack of intrinsic chiral preferences associated with the nanotube caps, as deduced from Figure [5], warrants the exploration of other routes towards χ-control. A possible, expedient approach might rest upon the theoretical scheme proposed in Ref.[29] that allowed us to quantify the energetics of graphene edge and, in particular, the sp^2-carbon–metal interface.[4, 29, 53] The chemical aspect to an interface-controlled scenario is that unlike the "chirally inert" capped end of a CNT, the open-edge (see inset in Figure [1]) energy is χ-dependent,[29]

$$\gamma(\chi) = 2\gamma_{AC} \sin\chi + 2\gamma_{ZZ} \sin(\pi/6 - \chi)$$
$$= |\gamma|\cos(\chi + C), \qquad (8)$$

and can be fine-tuned ultimately through the chemical "phase shift" $C = C(\mu)$, μ being the chemical potential of the species in contact with the edge. Combining eq. 8 with eq. [3], one obtains the total excess energy of a capped CNT with a chemically modified open edge, $\Omega(d,\chi) + \Gamma(d,\chi)$, where $\Gamma(d,\chi) \equiv \pi d\,\gamma(\chi)$. The effect of different edge terminations is illustrated in Figure [6]. The "distortion" of the reference (dashed) isoenergy contours, corresponding to the analytical surface in Figure [5], is a simple consequence of the term $\sim d \times \cos\chi$. In this case the $\Omega(d,\chi)$ surface is obtained by irregular-grid interpolation of the actual calculated points which leads to a generally "rough" surface and thereby wiggled isoenergy contours. Note, however, that the dominant effect comes from the edge term, viz. the nature of the species in contact with the open CNT edge. Thus, within the thermodynamic arguments of Ref.[29], Co and Fe would render ZZ-edge preference, while hydrogen results in preferred AC edge.
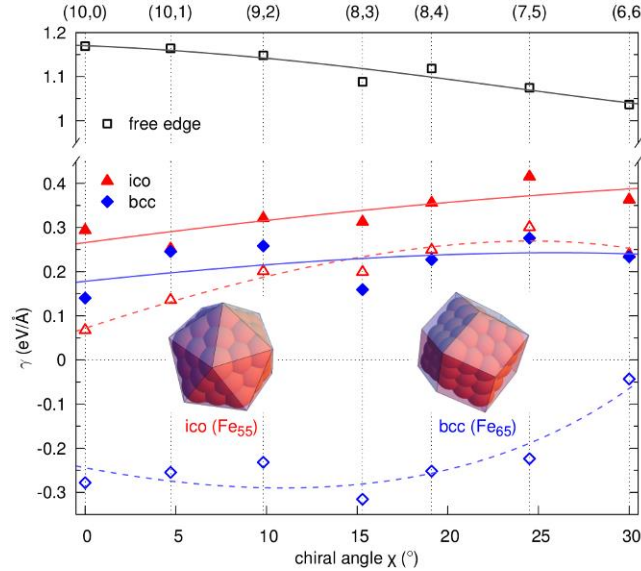

Figure 7: Comparison of the absolute CNT/catalyst interface energies $\gamma(\chi)$ (symbols) of smaller-diameter tubes, cf. Fig. [2], for a free edge and in contact with two Fe clusters of different shapes: an icosahedral Fe_{55} cluster (left image), and a rhombic dodecahedral bcc-Fe_{65} cluster (right image), as calculated with DF-TB. Open symbols correspond to values calculated without spin polarization. The lines are least-square fits to the analytical expression, eq. 8, also including a ZZ–AC mixing term.[29]

The dominant role of the CNT/catalyst interface can be illustrated by direct atomistic calculations of $\gamma(\chi)$ (see Methods section for details). For that purpose, we use the identified lowest-energy caps, corresponding to the set of chiralities from Figure [2], and arrange them for comparison on two Fe clusters of different shape: an icosahedral Fe_{55} cluster and a Fe_{65} rhombic dodecahedron with a body-centered cubic (bcc) structure, Figure [7]. $\gamma(\chi)$ of the individual free-edge tubes (essentially that of the pristine graphene edge[29]) is given as a reference, showing the familiar trend with preferred AC edge. On a Fe_n

8

cluster this trend is reversed, as already seen in Figure 6. This example, using a *monoelemental* cluster, shows that the catalyst shape and magnetic state provide additional routes towards control of $\gamma(\chi)$. It is worth noting that for an assumed non-magnetic state of the Fe_{65} cluster, the combined effect of the AC–ZZ mixing term and phase shift C leads to a convex $\gamma(\chi)$ and a negative interface energy,[29] with a local minimum in the center of the 30° chirality window. For the magic-size icosahedral Fe_{55} cluster the magnetic state reflects merely in a constant shift for all but the ZZ interface.

Conclusions

Single-walled CNT are now routinely grown and chirality distribution maps are abundant in the literature.[54-65] Chronologically, those experimental works seem to reveal a gradually emerging chiral selectivity, with some of the most recent experiments demonstrating unusually strong, and eventually puzzling, preference towards near-armchair CNTs.[54, 55] Controlling the caps structure, and hence their energetics, has been deemed a possible route toward chiral selectivity in catalytic growth of CNTs. To provide rigorous quantitative basis for analysis, here we have presented a detailed mapping of the intrinsic elastic energy landscape of capped single-walled CNTs. The explicit account of multiple structural isomers (i.e., the configurational variety of the six-pentagon pattern of the caps) essentially proves no viable correlation between the cap energetics and the chiral angle χ. Thus, the "end-caps" of a carbon nanotube do not display an intrinsic preference to a specific chirality (n,m) which leaves room for other approaches to control the chirality, especially by tuning the interaction between nanotube edge and catalyst[29] via the choice of material, catalyst shape, and possibly other state characteristics. The present work also provides valuable information for the analysis of properties where the details in the pentagonal pattern of the CNT end-cap are essential and have major imprint on its electronic structure.[66-69]

Methods

Enumeration of all possible isolated-pentagon caps for given (n,m) and generation of the corresponding atomic coordinates were performed with the Chemical and abstract graph environment CAGE.[70] The two-dimensional graphs output by CAGE were postprocessed by HYPERCHEM software[71] to generate the initial three-dimensional Cartesian coordinates of the structures for subsequent optimization in other codes as explained below. The total number of caps generated was $N^{cap} = 4548$. Each final geometry represents the CNT cap along with three "layers" of hexagons from the nascent nanotube. Closed, fullerene *cages* were constructed from the single-cap (or "half-tube") geometries by duplication (therefore twice bigger number of atoms in the cage) followed by appropriate set of coordinate transformations.

Total energies were calculated within density-functional theory (DFT) using the SIESTA[72] code, the density-functional based tight binding method (DF-TB) using the DFTB+ code,[73] and employing the AIREBO/REBO reactive bond-order empirical potentials[74, 75] as implemented in the LAMMPS[76] simulator.

The DFT calculations were carried out using the PBE generalized gradient approximation functional[77] with a localized pseudoatomic orbital (double-ζ, polarized) basis set and Troullier–Martins norm-conserving pseudopotentials. The simulation cell was chosen so as to ensure at least 1 nm vacuum region between system images in a nonperiodic direction. For CNT calculations, Brillouin zone sampling along the axis was chosen so that the corresponding effective spatial cutoff was within the range of 8–11 nm for all tubes. Conjugate gradient scheme with force tolerance 0.01 eV/Å was used to optimize all geometries.

The self-consistent charge DF-TB calculations employ Slater–Koster parameters as provided in the `pbc-0-3`[78] and `trans3d-0-1`[79] sets. The CNT/catalyst interface energy in Figure 7 is defined as $\gamma = (E^{tot} -$

$\frac{1}{2} E_{n,m}{}^{\text{tot}} - E_{\text{Fe}})/\pi d$, where E^{tot} is the energy of the CNT/Fe$_n$ system, E_{Fe} – the energy of the free Fe$_n$ cluster, and $E_{n,m}{}^{\text{tot}}$ – the energy of the closed CNT cage with minimal $\Omega_{n,m}$, for given (n,m), eq. 3. The CNT axis in the initial geometry is along the five-fold axis of the icosahedral Fe$_{55}$ cluster, and along the three-fold axis of the dodecahedral Fe$_{65}$ cluster, respectively. Conjugate gradient optimization is performed with force tolerance of 0.05 eV/Å. Spin-polarized calculations are performed first for isolated cluster to determine the net magnetic moments. For the icosahedral Fe$_{55}$ we reproduce the value 1.93 μ_B/atom (antiferromagnetic state) from Ref.[80], while the calculated magnetic moment for the bcc Fe$_{65}$ cluster (ferromagnetic state) is 2.8 μ_B/atom. Geometry optimization of the CNT/Fe$_n$ systems is performed keeping the magnetic moments on the Fe$_n$ cluster collinear, setting the initial net values according to those determined for the isolated cluster.

The procedure for calculating the energetics of the larger caps for $d \approx 1$ nm, due to their huge number, differs slightly from the one described above for the smaller-diameter tubes. All caps were optimized at all but the DFT level, using the as-generated[70] "half-tube" geometries. To subtract the energy contribution due to the open edge, an additional set of calculations has been carried out for long, *finite* CNTs with exactly the same edges as the caps. The edge structure of all half-tubes was parsed/verified with our EDGECOUNT tool.[81] As a second step, closed cages were generated only from the ten half-tubes with lowest $\Omega_{n,m}$ for each chiral angle (only these $9 \times 10 = 90$ closed-cage structures were calculated with DFT). To calculate various graph characteristics, we use the algorithm from Ref.[82] that implements the nilpotent adjacency matrix method for enumerating pentagonal and hexagonal cycles in the cap graphs.

References to Section I

1.   Iijima, S., Helical microtubules of graphitic carbon. *Nature* **1991,** *354*, 56-58.
2.   Jin, C.; Suenaga, K.; Iijima, S., How does a carbon nanotube grow? An in situ investigation on the cap evolution. *ACS Nano* **2008,** *2*, 1275-1279.
3.   Nesterenko, A. M.; Kolesnik, N. F.; Akhmatov, Y. S.; Suhomlin, V. I.; Prilutskii, O. V., Specifics of the phase composition and products of the NiO and Fe$_2$O$_3$ reaction with carbon monoxide. *Izv. Akad. Nauk SSSR, Met.* **1982,** *3*, 12-17.
4.   Penev, E. S.; Artyukhov, V. I.; Ding, F.; Yakobson, B. I., Unfolding the Fullerene: Nanotubes, Graphene and Poly-Elemental Varieties by Simulations. *Adv. Mater.* **2012,** *24*, 4956-4976.
5.   Pigos, E.; Penev, E. S.; Ribas, M. A.; Sharma, R.; Yakobson, B. I.; Harutyunyan, A. R., Carbon Nanotube Nucleation Driven by Catalyst Morphology Dynamics. *ACS Nano* **2011,** *5* (12), 10096-10101.
6.   Schebarchov, D.; Hendy, S. C.; Ertekin, E.; Grossman, J. C., Interplay of Wetting and Elasticity in the Nucleation of Carbon Nanotubes. *Phys. Rev. Lett.* **2011,** *107*, 185503-185503.
7.   Ohta, Y.; Okamoto, Y.; Page, A. J.; Irle, S.; Morokuma, K., Quantum Chemical Molecular Dynamics Simulation of Single-Walled Carbon Nanotube Cap Nucleation on an Iron Particle. *ACS Nano* **2009,** *3*, 3413-3420.
8.   Ribas, M. A.; Ding, F.; Balbuena, P. B.; Yakobson, B. I., Nanotube nucleation versus carbon-catalyst adhesion--Probed by molecular dynamics simulations. *J. Chem. Phys.* **2009,** *131*, 224501-224501.
9.   Moors, M.; Amara, H.; Visart de Bocarmé, T.; Bichara, C.; Ducastelle, F.; Kruse, N.; Charlier, J. C., Early stages in the nucleation process of carbon nanotubes. *ACS Nano* **2009,** *3*, 511-516.
10.   Amara, H.; Bichara, C.; Ducastelle, F., Understanding the nucleation mechanisms of carbon nanotubes in catalytic chemical vapor deposition. *Phys. Rev. Lett.* **2008,** *100*, 56105-56105.
11.   Wells, J. C.; Noid, D. W.; Sumpter, B. G.; Wood, R. F.; Zhang, Q., Multiscale Simulations of Carbon Nanotube Nucleation and Growth: Electronic Structure Calculations. *J. Nanosci. Nanotech.* **2004,** *4*, 414-422.
12.   Fan, X.; Buczko, R.; Puretzky, A. A.; Geohegan, D. B.; Howe, J. Y.; Pantelides, S. T.; Pennycook, S. J., Nucleation of single-walled carbon nanotubes. *Phys. Rev. Lett.* **2003,** *90*, 145501-145501.
13.   Zhang, P.; Crespi, V. H., Nucleation of carbon nanotubes without pentagonal rings. *Phys. Rev. Lett.* **1999,** *83*, 1791-1794.
14.   Krishnan, A.; Dujardin, E.; Treacy, M. M. J.; Hugdahl, J.; Lynum, S.; Ebbesen, T. W., Graphitic cones and the nucleation of curved carbon surfaces. *Nature* **1997,** *388*, 451-454.
15.   Kuznetsov, V. L.; Usoltseva, A. N.; Chuvilin, A. L.; Obraztsova, E. D.; Bonard, J. M.,

Thermodynamic analysis of nucleation of carbon deposits on metal particles and its implications for the growth of carbon nanotubes. *Phys. Rev. B* **2001,** *64*, 235401-235401.

16. Gao, J.; Yip, J.; Zhao, J.; Yakobson, B. I.; Ding, F., Graphene Nucleation on Transition Metal Surface: Structure Transformation and Role of the Metal Step Edge. *J. Am. Chem. Soc.* **2011,** *133*, 5009-5015.

17. Wang, B.; Ma, X.; Caffio, M.; Schaub, R.; Li, W. X., Size-Selective Carbon Nanoclusters as Precursors to the Growth of Epitaxial Graphene. *Nano Lett.* **2011,** *11*, 424-430.

18. Lacovig, P.; Pozzo, M.; Alfe, D.; Vilmercati, P.; Baraldi, A.; Lizzit, S., Growth of dome-shaped carbon nanoislands on Ir (111): the intermediate between carbidic clusters and quasi-free-standing graphene. *Phys. Rev. Lett.* **2009,** *103*, 166101-166101.

19. Yuan, Q.; Gao, J.; Shu, H.; Zhao, J.; Chen, X.; Ding, F., Magic Carbon Clusters in the Chemical Vapor Deposition Growth of Graphene. *J. Am. Chem. Soc.* **2011**.

20. Singh, A. K.; Penev, E. S.; Yakobson, B. I., Vacancy clusters in graphane as quantum dots. *ACS Nano* **2010,** *4*, 3510-3514.

21. Lin, Y.; Ding, F.; Yakobson, B. I., Hydrogen storage by spillover on graphene as a phase nucleation process. *Phys. Rev. B* **2008,** *78*, 041402-041402.

22. Liu, Y.; Yakobson, B. I., Cones, Pringles, and Grain Boundary Landscapes in Graphene Topology. *Nano Lett.* **2010,** *10*, 2178-2183.

23. Kanzow, H.; Lenski, C.; Ding, A., Single-wall carbon nanotube diameter distributions calculated from experimental parameters. *Phys. Rev. B* **2001,** *63*, 125402-125402.

24. Tersoff, J., Energies of fullerenes. *Phys. Rev. B* **1992,** *46*, 15546-15546.

25. Šiber, A., Energies of sp^2 carbon shapes with pentagonal disclinations and elasticity theory. *Nanotechnology* **2006,** *17*, 3598-3598.

26. Nasibulin, A. G.; Pikhitsa, P. V.; Jiang, H.; Kauppinen, E. I., Correlation between catalyst particle and single-walled carbon nanotube diameters. *Carbon* **2005,** *43*, 2251-2257.

27. Zhang, Y.; Li, Y.; Kim, W.; Wang, D.; Dai, H., Imaging as-grown single-walled carbon nanotubes originated from isolated catalytic nanoparticles. *Appl. Phys. A* **2002,** *74*, 325-328.

28. Fiawoo, M. F. C.; Bonnot, A. M.; Amara, H.; Bichara, C.; Thibault-Pénisson, J.; Loiseau, A., Evidence of Correlation between Catalyst Particles and the Single-Wall Carbon Nanotube Diameter: A First Step towards Chirality Control. *Phys. Rev. Lett.* **2012,** *108*, 195503-195503.

29. Liu, Y.; Dobrinsky, A.; Yakobson, B. I., Graphene Edge from Armchair to Zigzag: The Origins of Nanotube Chirality? *Phys. Rev. Lett.* **2010,** *105*, 235502-235502.

30. Reich, S.; Li, L.; Robertson, J., Control the chirality of carbon nanotubes by epitaxial growth. *Chem. Phys. Lett.* **2006,** *421*, 469-472.

31. Reich, S.; Li, L.; Robertson, J., Structure and formation energy of carbon nanotube caps. *Phys. Rev. B* **2005,** *72*, 165423-165423.

32. Reich, S.; Li, L.; Robertson, J., Epitaxial growth of carbon caps on Ni for chiral selectivity. *phys. stat. sol. (b)* **2006,** *243*, 3494-3499.

33. Lair, S. L.; Herndon, W. C.; Murr, L. E.; Quinones, S. A., End cap nucleation of carbon nanotubes. *Carbon* **2006,** *44*, 447-455.

34. Gómez-Gualdrón, D. A.; Balbuena, P. B., The role of cap chirality in the mechanism of growth of single-wall carbon nanotubes. *Nanotechnology* **2008,** *19*, 485604-485604.

35. Zhao, J.; Balbuena, P. B., Effect of Nanotube Cap on the Aromaticity of Single-Wall Carbon Nanotubes. *J. Phys. Chem. C* **2008,** *112* (34), 13175-13180.

36. Wang, Q.; Ng, M. F.; Yang, S. W.; Yang, Y.; Chen, Y., The mechanism of single-walled carbon nanotube growth and chirality selection induced by carbon atom and dimer addition. *ACS Nano* **2010,** *4*, 939-946.

37. Zhu, W.; Börjesson, A.; Bolton, K., DFT and tight binding Monte Carlo calculations related to single-walled carbon nanotube nucleation and growth. *Carbon* **2010,** *48*, 470-478.

38. Brinkmann, G.; Fowler, P. W.; Manolopoulos, D. E.; Palser, A. H. R., A census of nanotube caps. *Chemi. Phys. Lett.* **1999,** *315*, 335-347.

39. Dresselhaus, M. S.; Dresselhaus, G.; Eklund, P. C., *Science of Fullerenes and Carbon Nanotubes*. Academic Press: 1996.

40. Dresselhaus, M. S.; Dresselhaus, G.; Saito, R., Physics of carbon nanotubes. *Carbon* **1995,** *33*, 883-891.

41. Delgado Friedrichs, O.; Dress, A. W. M.; Huson, D. H.; Klinowski, J.; Mackay, A. L., Systematic enumeration of crystalline networks. *Nature* **1999,** *400*, 644-647.

42. Mackay, A. L., From "The Dialectics of Nature" to the Inorganic Gene. *Found. Chem.* **1999,** *1*, 43-56.

43.   Brinkmann, G.; Nathusius, U. v.; Palser, A. H. R., A constructive enumeration of nanotube caps. *Discr. Appl. Math.* **2002,** *116*, 55-71.

44.   Adams, G. B.; Sankey, O. F.; Page, J. B.; O'Keeffe, M.; Drabold, D. A., Energetics of large fullerenes: balls, tubes, and capsules. *Science* **1992,** *256*, 1792-1795.

45.   Robertson, D. H.; Brenner, D. W.; Mintmire, J. W., Energetics of nanoscale graphitic tubules. *Phys. Rev. B* **1992,** *45* (21), 12592-12595.

46.   Sawada, S.; Hamada, N., Energetics of carbon nano-tubes. *Solid State Commun.* **1992,** *83* (11), 917-919.

47.   Tománek, D.; Zhong, W.; Krastev, E., Stability of multishell fullerenes. *Phys. Rev. B* **1993,** *48*, 15461-15464.

48.   Muñoz, E.; Singh, A. K.; Ribas, M. A.; Penev, E. S.; Yakobson, B. I., The ultimate diamond slab: GraphAne versus graphEne. *Diam. Relat. Mater.* **2010,** *19*, 368-373.

49.   Cross, S.; Kuttel, M. M.; Stone, J. E.; Gain, J. E., Visualisation of cyclic and multi-branched molecules with VMD. *J. Mol. Graph. Model.* **2009,** *28*, 131-139.

50.   Humphrey, W.; Dalke, A.; Schulten, K., VMD -- Visual Molecular Dynamics. *J. Mol. Graph.* **1996,** *14*, 33-38.

51.   Fowler, P. W.; Caporossi, G.; Hansen, P., Distance matrices, Wiener indices, and related invariants of fullerenes. *J. Phys. Chem. A* **2001,** *105*, 6232-6242.

52.   Kudin, K. N.; Scuseria, G. E.; Yakobson, B. I., C$_2$F, BN, and C nanoshell elasticity from ab initio computations. *Phys. Rev. B* **2001,** *64*, 235406-235406.

53.   Artyukhov, V. I.; Liu, Y.; Yakobson, B. I., Equilibrium at the edge and atomistic mechanisms of graphene growth. *Proc. Natl. Acad. Sci. USA* **2012,** *109* (38), 15136-15140.

54.   Wang, H.; Wei, L.; Ren, F.; Wang, Q.; Pfefferle, L. D.; Haller, G. L.; Chen, Y., Chiral-Selective CoSO$_4$/SiO$_2$ Catalyst for (9,8) Single-Walled Carbon Nanotube Growth. *ACS Nano* **2013,** *7*, 614-626.

55.   He, M.; Jiang, H.; Liu, B.; Fedotov, P. V.; Chernov, A. I.; Obraztsova, E. D.; Cavalca, F.; Wagner, J. B.; Hansen, T. W.; Anoshkin, I. V.; Obraztsova, E. A.; Belkin, A. V.; Sairanen, E.; Nasibulin, A. G.; Lehtonen, J.; Kauppinen, E. I., Chiral-Selective Growth of Single-Walled Carbon Nanotubes on Lattice-Mismatched Epitaxial Cobalt Nanoparticles. *Sci. Rep.* **2013,** *3*, 1460-1460.

56.   Fouquet, M.; Bayer, B. C.; Esconjauregui, S.; Blume, R.; Warner, J. H.; Hofmann, S.; Schlögl, R.; Thomsen, C.; Robertson, J., Highly chiral-selective growth of single-walled carbon nanotubes with a simple monometallic Co catalyst. *Phys. Rev. B* **2012,** *85*, 235411-235411.

57.   Zhu, Z.; Jiang, H.; Susi, T.; Nasibulin, A. G.; Kauppinen, E. I., The Use of NH$_3$ to Promote the Production of Large-Diameter Single-Walled Carbon Nanotubes with a Narrow (n,m) Distribution. *J. Am. Chem. Soc.* **2011,** *133*, 1224-1227.

58.   Kato, T.; Hatakeyama, R., Direct Growth of Short Single-Walled Carbon Nanotubes with Narrow-Chirality Distribution by Time-Programmed Plasma Chemical Vapor Deposition. *ACS Nano* **2010,** *4*, 7395-7400.

59.   Wijeratne, S. S.; Harris, N. C.; Kiang, C. H., Helicity Distributions of Single-Walled Carbon Nanotubes and Its Implication on the Growth Mechanism. *Materials* **2010,** *3*, 2725-2734.

60.   Fouquet, M.; Hofmann, S.; Thomsen, C.; Robertson, J., Analysis of carbon nanotube chiralities obtained from a bimetallic Co-Mo catalyst. *phys. status solidi (b)* **2010,** *247*, 2660-2663.

61.   Chiang, W. H.; Sakr, M.; Gao, X. P. A.; Sankaran, R. M., Nanoengineering Ni$_x$Fe$_1-x$ Catalysts for Gas-Phase, Selective Synthesis of Semiconducting Single-Walled Carbon Nanotubes. *ACS Nano* **2009,** *3* (12), 4023-4032.

62.   Chiang, W. H.; Sankaran, R. M., Linking catalyst composition to chirality distributions of as-grown single-walled carbon nanotubes by tuning Ni$_x$Fe$_1-x$ nanoparticles. *Nat. Mater.* **2009,** *8*, 882-886.

63.   Bachilo, S. M.; Balzano, L.; Herrera, J. E.; Pompeo, F.; Resasco, D. E.; Weisman, R. B., Narrow (n,m)-Distribution of Single-Walled Carbon Nanotubes Grown Using a Solid Supported Catalyst. *J. Am. Chem. Soc.* **2003,** *125* (37), 11186-11187.

64.   Jorio, A.; Saito, R.; Hafner, J. H.; Lieber, C. M.; Hunter, M.; McClure, T.; Dresselhaus, G.; Dresselhaus, M. S., Structural (n,m) Determination of Isolated Single-Wall Carbon Nanotubes by Resonant Raman Scattering. *Phys. Rev. Lett.* **2001,** *86*, 1118-1121.

65.   Sato, Y.; Yanagi, K.; Miyata, Y.; Suenaga, K.; Kataura, H.; Iijima, S., Chiral-angle distribution for separated single-walled carbon nanotubes. *Nano Lett.* **2008,** *8*, 3151-3154.

66.   Marchand, M.; Journet, C.; Guillot, D.; Benoit, J. M.; Yakobson, B. I.; Purcell, S. T., Growing a Carbon Nanotube Atom by Atom: "And Yet It Does Turn". *Nano Lett.* **2009,** *9*, 2961-2966.

67.   Khazaei, S.; Khazaei, M.; Cheraghchi, H.; Daadmehr, V.; Kawazoe, Y., Considering the effect of

different arrangements of pentagons on density of states of capped carbon nanotubes. *Physica B* **2011,** *406*, 3885-3890.

68.		Carroll, D. L.; Redlich, P.; Ajayan, P. M.; Charlier, J. C.; Blase, X.; De Vita, A.; Car, R., Electronic Structure and Localized States at Carbon Nanotube Tips. *Phys. Rev. Lett.* **1997,** *78*, 2811-2814.

69.		Khazaei, M.; Dean, K. A.; Farajian, A. A.; Kawazoe, Y., Field Emission Signature of Pentagons at Carbon Nanotube Caps. *J. Phys. Chem. C* **2007,** *111* (18), 6690-6693.

70.		Brinkmann, G.; Delgado Friedrichs, O.; Lisken, S.; Peeters, A.; Van Cleemput, N., CaGe - a Virtual Environment for Studying Some Special Classes of Plane Graphs - an Update. *MATCH Commun. Math. Comput. Chem.* **2010,** *63*, 533-552.

71.		*HyperChem(TM) Professional 7.51*, Hypercube, Inc.

72.		Soler, J. M.; Artacho, E.; Gale, J. D.; Garcia, A.; Junquera, J.; Ordejón, P.; Sánchez-Portal, D., The SIESTA method for ab initio order-N materials simulation. *J. Phys.: Cond. Matter* **2002,** *14*, 2745-2779.

73.		Aradi, B.; Hourahine, B.; Frauenheim, T., DFTB+, a Sparse Matrix-Based Implementation of the DFTB Method. *J. Phys. Chem. A* **2007,** *111* (26), 5678-5684.

74.		Brenner, D. W.; Shenderova, O. A.; Harrison, J. A.; Stuart, S. J.; Ni, B.; Sinnott, S. B., A second-generation reactive empirical bond order (REBO) potential energy expression for hydrocarbons. *J. Phys.: Condens. Matter* **2002,** *14*, 783-802.

75.		Stuart, S. J.; Tutein, A. B.; Harrison, J. A., A reactive potential for hydrocarbons with intermolecular interactions. *J. Chem. Phys.* **2000,** *112*, 6472-6486.

76.		Plimpton, S. J., Fast Parallel Algorithms for Short-Range Molecular Dynamics. *J. Comp. Phys.* **1995,** *117*, 1-19.

77.		Perdew, J. P.; Burke, K.; Ernzerhof, M., Generalized gradient approximation made simple. *Phys. Rev. Lett.* **1996,** *77*, 3865-3868.

78.		Porezag, D.; Frauenheim, T.; Köhler, T.; Seifert, G.; Kaschner, R., Construction of tight-binding-like potentials on the basis of density-functional theory: Application to carbon. *Phys. Rev. B* **1995,** *51*, 12947-12957.

79.		Zheng, G.; Witek, H. A.; Bobadova-Parvanova, P.; Irle, S.; Musaev, D. G.; Prabhakar, R.; Morokuma, K.; Lundberg, M.; Elstner, M.; Köhler, C.; Frauenheim, T., Parameter calibration of transition-metal elements for the spin-polarized self-consistent-charge density-functional tight-binding (DFTB) method: Sc, Ti, Fe, Co, and Ni. *J. Chem. Theory Comput.* **2007,** *3*, 1349-1367.

80.		Köhler, C.; Seifert, G.; Frauenheim, T., Magnetism and the potential energy hypersurfaces of Fe$\_53$ to Fe$\_57$. *Comp. Mater. Sci.* **2006,** *35* (3), 297-301.

81.		Singh, A. K.; Penev, E. S.; Yakobson, B. I., Armchair or Zigzag? A tool for characterizing graphene edge. *Comput. Phys. Comm.* **2011,** *182*, 804-807.

82.		Schott, R.; Staples, G. S., On the Complexity of Cycle Enumeration for Simple Graphs. In *Guide to Geometric Algebra in Practice*, Dorst, L.; Lasenby, J., Eds. Springer: 2011; pp 233-249.

II. Equilibrium at the edge and atomistic mechanisms of graphene growth

We completed the first "release" of our quantitative *nanoreactor diagram* (or model), based on the analysis of the nanotube or graphene edge atomistics. Through detailed description of the catalyst-carbon interface, defects energies, and growth rate, this approach makes predictions of nanotube distribution or graphene sheet shape, verifiable experimentally. Important findings in experimental growth provide strong support to the nanoreactor approach. This allowed us to readily calculate the rate of nanotube or graphene growth, on different catalyst metals such as Fe, Ni, Co, Cu. We also completed our study of *cooperative behavior* in growth of nanotube forests, their simulated kinetics with the account for the lateral forces and how such feedback results in the uniformity of carpet-growth. Found analytical equation establishes for the first time the average growth speed for an array on interlinked SWNT, or for a MWNT composed from a nested set with different chiralities. Details of this effort are fully available as published [1].

References to Section II

[1] "Equilibrium at the edge and atomistic mechanisms of graphene growth", V.I. Artyukhov, Y. Liu, and B.I. Yakobson, **Proc. Natl. Acad. Sci.**, 109, 15136-15140 (2012).

III. Lateral force feedback in growth of carbon nanotube arrays

Dislocation theory of *single wall* carbon nanotube (CNT) suggests a linear dependence between its chiral angle and growth speed[1]. However, CNTs normally grow in the form of *bundles* or *multi-walls* (MWNT), which tend to end up with roughly the same length at same time[2,3], indicating roughly same growth speed for different chiralities. Motivated by the apparent discrepancy between dislocation theory and experiments, we study the effect of interactions between CNTs on their growth. Van der Waals force, as the main interaction in our model, can slow down the fast-growing CNTs while speed up the slower ones between immediate neighbors. Our analytical equation and numerical simulations show that while two shells in a double-wall nanotube (DWNT) grow relatively independently at small diameters, they become inseparable for all non-zero chiral angles as their diameter approach 3nm under 800°C and deposition by atom reaction condition. Lacks of the cap effect, CNTs in bundles are susceptible to breaking down to separated growing domains under same condition. Nevertheless, as temperature decreases or as the precursor becomes carbon dimer or polymer, separated growing domains merge and form larger domains. We also found that within any domain in bundle and MWNT, all CNTs jointly grow at a speed proportional to an adjusted geometric mean of their chiral angles.

ARBON NANOTUBE (CNT) GROWTH, traditionally referring to synthesis of CNT, remains a great research challenge Cdespite tremendous effort [1,4,5,6,7]. Crystal morphology study suggests CNTs are produced in seemingly random diameter and chirality, often specified by a chiral angle χ between the circumference and the zigzag motif of atoms [1]. Dislocation theory examines CNT crystal structure and proposed a linear relation between the growth speed and the chiral angle of single wall nanotube (SWNT) [1]. Chemical vapor deposition (CVD) has become a major CNT synthesis method because of its potential in scalable mass synthesis of CNTs [8] and some potential applications of CNTs include sensors [9,10], super-capacitors [11], fuel cells [12], thermal conducting electronic circuit [13] and nano-rods [14,15]. However, nanotubes grown by CVD are often densely packed, aligned, and in forms of bundles or multi-walls. In contrast to dislocation theory prediction, many experiments have observed similar CNT growth speed on nanotubes in bundles and on nanotube shells within one MWNT [1,2]. This apparent discrepancy suggests a missing piece of our understanding in nanotube growth mechanism and our interests are in finding it.

Diffusion limitation and van der Waals interactions are two initial candidates. We rule out diffusion limitation because it does not sufficiently explain the speed consistency across nanotubes in large global domain (e.g. a CNT carpet) or in small local region with distinct chiral angles. On the other hand, many researchers have studied van der Waals interaction between nanotubes and graphite [16 - 18], but people haven't associated van der Waals interaction with nanotube growth reaction kinetics. In the following, we explore the effect of van der Waals interactions on the nanotube growth speed and introduce a length-speed feedback mechanism bridging the dislocation theory and experimental observations.

The Lennard-Jones (LJ) potential for two atoms with x distance apart is

$$u(x) = -\frac{A}{x^6} + \frac{B}{x^{12}} \qquad (1)$$

The equilibrium distance is given by

$$x_0 = \left(\frac{2B}{A}\right)^{\frac{1}{2}} \qquad (2)$$

Any deviation from this equilibrium distance will result in an increase in potential energy. At any instance during growth process, the carbon precursor is more likely to deposit onto the tube where it can minimize the overall LJ potential of the system.

Carbon nanotube dislocation theory, proposed by Feng Ding, shows that growth speed of a

single CNT must be proportional to the magnitude of its chiral angle,

$$K \propto \chi \cdot k_0,\qquad(3)$$

where K is the growth speed in length per unit time, χ is the chiral angle and k_0 is some rate constant [1].
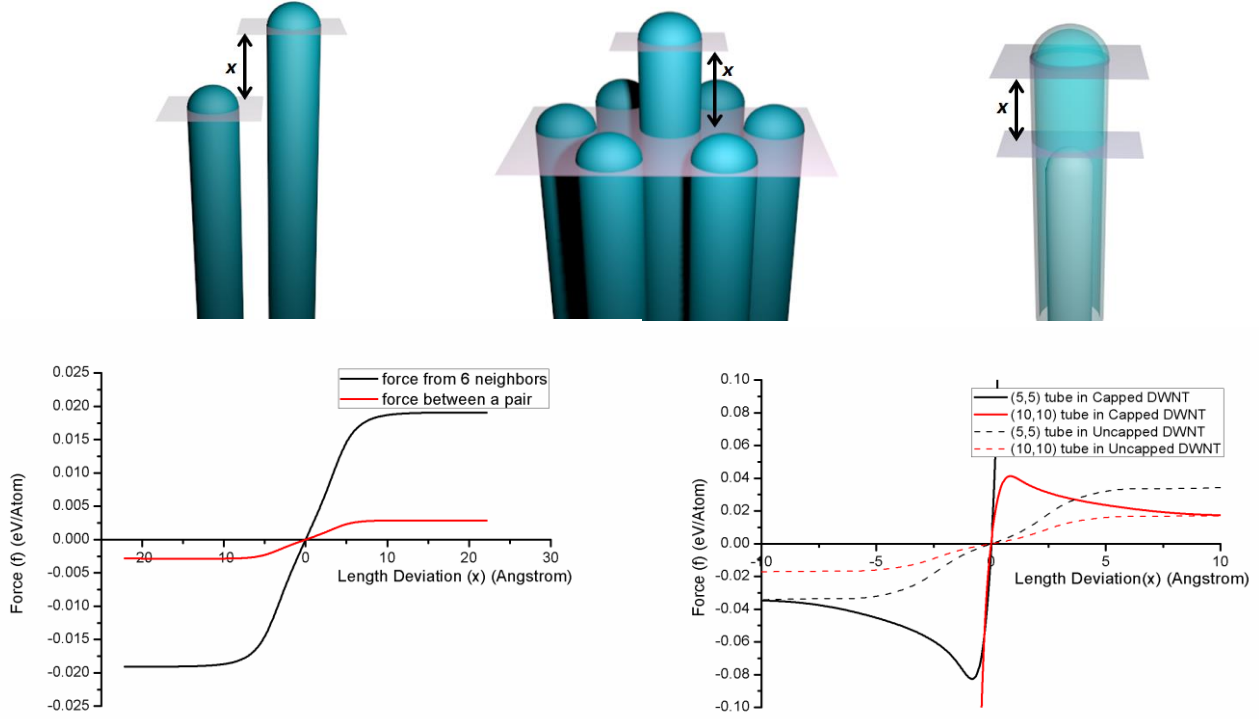
According to *Arrhenius equation*, k_0 in eq.(1) must be proportional to reaction rate constant r,

$$k_0 \propto r = A e^{\frac{-E_A^\circ - p\Delta V}{kT}} \sim e^{\frac{-E_A^\circ - \hat{f}\Delta l}{kT}}\qquad(4)$$

Here, we assume that the nanotube van der Waals force on carbon precursor contributes to the reaction rate by adding a bias energy $-\hat{f}\Delta l$ (equivalent to $-p\Delta V$) to a constant activation energy component E_A° in the exponential. Δl is some length increment. We view that a tube grows with precursor units discretely depositing on it. After each deposition, the tube gains Δn atoms. For our purpose, we use discrete force notation f in unit of eV/atom in the following discussion. $f\Delta n = \hat{f}\Delta l$, where Δn is the carbon atom number increment and the $\frac{\Delta l}{\Delta n}$ ratio depends on the diameter of the tube.

We construct three models (shown in Fig. 1. a, b ,c) and an uncapped double-wall nanotube

15

(DWNT) model to study the interaction force originated from small tube length deviation by molecular dynamics simulation.

In tube pair model Fig. 1. a, the length deviation of tube i is defined as $x_{i,j} = L_i - L_j = -x_{j,i}$, where j indexes the neighbor tube of tube i. Similarly, in Fig. 1. b where six peripheral tubes are held static, the length deviation is $x = L_{center} - L_{periphery}$. In DWNT model (Fig. 1. c), $x_{i,j} = 0$ is defined at the equilibrium separation between two caps. $x_{i,j} = (L_i - \epsilon) - L_j = -x_{j,i}$, where j indexes the inner shell, i indexes the outer shell and ϵ is the equilibrium cap separation.

According to Newton's law, in the symmetric pair model (Fig. 1. a) we have

$$f_i(x_{i,j}) = -f_j(x_{j,i}) = -f_i(-x_{i,j}) \qquad (5)$$

where f_i is the force on tube i. In Fig. 1. c, two shells have different diameters and thus the eq. 5 becomes

$$f_i(x_{i,j}) = -f_j(x_{j,i}) \cdot \frac{d_j}{d_i} \qquad (6)$$

Here d_i, d_j are the diameters of tube i and j. In our notation, positive force is downward acting against growth and negative force is upward.

The force curves exhibit asymptotical symmetry, linearity and cap effect. Fig. 1. d depicts the forces measured in tube pair (model a) and seven tube bundle (model b). The forces follow an arctangent shape. The magnitude of the force between a pair as x goes to infinity is $2.85 \times 10^{-3} eV/atom$, which agrees with Girifalco's paper to the order of $10^{-4} \, eV/atom$ [16]. The force measured from the center tube with six neighbors is about 6 times larger than the force from model a, indicating $f_{bundle}(x) = \Sigma_{j=1}^{6} f_j(x) = 6f_{pair}(x)$, where f_j denotes the force contribution from the j-th neighbor on periphery. In an uncapped DWNT, the forces between two cylindrical shells are close to the force measured from center tube with six neighbors. Nevertheless, the forces computed from capped shells (shown in Fig. 1. c and e) differ from the uncapped model in two major ways: first, the magnitude of force goes to infinity when the distance between two caps is less than ϵ, suggesting that inner tube penetration through outer shell is prohibited; second, the magnitude of force increases sharply at small length deviations acting against cap separation, but as caps further separate, this cap effect gradually diminishes and the force curves converge with those from uncapped model.

Cap effect in MWNT increases linearly with the diameter of the inner shell. Cap effect results from a fast change of LJ potential energy between two CNT caps. The magnitude of this energy change is proportional to the number of atoms on the caps. We assume the area of the inner cap is the determining factor of maximum cap effect for analysis simplicity. The cap effect between any pair is approximately proportional to the surface area of the inner cap. Therefore at a given cap separation, the potential energy change between caps is $\Delta E_{cap} \propto \pi r_{inner}^2$. The cap effect component on force is calculated by

$$f_{cap} = \frac{\Delta E_{cap}}{\Delta \hat{n}} \propto \frac{\pi r_{inner}^2}{2\pi r} \propto \frac{r_{inner}^2}{r} \qquad (7)$$

$\Delta \hat{n}$ is the number of atom increment necessary to achieve a separation between caps that

16

corresponds to the energy change ΔE_{cap}. r is the radius of the subject shell and r_{inner} is the radius of the inner shell. Because the radius of the outer shell is larger, we see a less significant cap effect on the outer shell in our DWNT simulation.

We integrate more comprehensive index and force notation into eq. 4, and the instant growth speed of tube i becomes,

$$K_i(t) = \chi_i \cdot A e^{\frac{-E_A^\circ - \sum_j f_{i,j}\Delta n}{kT}} \propto \chi_i e^{\frac{-\sum_j f_{i,j}\Delta n}{kT}} \qquad (8)$$

We denote the force from tube j to tube i as $f_{i,j}$ equaling to $f_i\left(x_{i,j}(t)\right)$. "$-\sum_j f_{i,j}\Delta n$" sums up the bias energy contributions from all neighbors of tube i at time t. In our model, a tube is either in a MWNT with 2 neighbor shells or in a CNT bundle with 6 neighbors.

In steady state growth, CNT growth speed is proportional to a geometric mean of the chiral angles of all jointly growing tube. Consider a simplest two tube scenario where we only have the interaction between two tubes, indexed as 1 and 2. According to eq. 7 and eq. 5, same growth speed $K_1(t) = K_2(t)$ can be achieved if $f_{1,2}$ is large enough such that,

$$\chi_1 e^{\frac{-f_{1,2}\Delta n}{kT}} = \chi_2 e^{\frac{-f_{2,1}\Delta n}{kT}} = \chi_2 e^{\frac{f_{1,2}\Delta n}{kT}} \qquad (9)$$

Algebra leads to the geometric mean solution,

$$\chi_e = \chi_1 e^{\frac{-f_{1,2}\Delta n}{kT}} = \chi_2 e^{\frac{f_{1,2}\Delta n}{kT}} = \sqrt{\chi_1 \chi_2} \qquad (10)$$

χ_e is the *equilibrium chiral coefficient* that is proportional to the joint growth speed. In a MWNT, $f_{1,2} = f_{wall} + f_{cap}$. Our simulation (Fig.1.e) shows $max(f_{1,2}) \approx max(f_{cap})$. Fitted eq. 7 with the simulation data, we have $max(f_{cap}) = \frac{0.016 r_{inner}^2}{r}$ eV/Atom (radius in unit of Å). From eq. 9 we can calculate the maximum chiral angle ratio between jointly growing pair that the force can sustain,

$$max\left(\frac{\chi_1}{\chi_2}\right) = e^{\frac{2 max(f_{1,2})\Delta n}{kT}} = e^{\frac{0.032 r_{inner}^2 \Delta n}{kT r}} \qquad (11)$$

At T = 1073K, $\Delta n = 1$ and $r_{inner} = r = 27$Å, $max\left(\frac{\chi_1}{\chi_2}\right) \approx 10^4$, which essentially means inseparable.

We expand the analysis to N adjacent tubes in a row or N shells in a MWNT and exclude the boundary effect for now. Algebra still leads to the geometric mean equilibrium chiral coefficient, $\chi_e = \sqrt{\chi_1 \chi_2 \cdots \chi_N}$. Actually by similar analysis on eq. 7 and eq. 5, we find χ_e to be the same geometrical mean of the chiral angles of all tubes within any arbitrary shape joint growth domains in densely packed bundles.

Equality in eq. 9 is not always achieved because the force has a maximum magnitude, and therefore has a maximum growth speed adjusting ability. Once $\frac{\chi_1}{\chi_2}$ exceeds $e^{\frac{2 f_{1,2}\Delta n}{kT}}$, two tubes will no longer grow jointly. Instead, they *break off* from each other and their length difference increase linearly with time. When adjacent tubes in MWNT or bundle break off, a boundary is created.

The boundary effect introduces a speed modifier to the equilibrium chiral coefficient. Any nanotube on the boundary of jointly growing domain grows either faster (an *up-break*) or slower (a *down-break*) than its break-off neighbor tubes. Sometimes, the jointly growing domain boundary is exposed to ambient space (e.g. largest diameter shell in MWNT). In our analysis, we treat an ambient space neighbor as a zero length CNT neighbor. The interaction force at large length deviation becomes a constant as the force curves converge. Therefore, we invoke a constant speed modifier to account for the force effect on boundary tube.

We define boundary *up-break* tube growth speed modifier as $\frac{1}{\Upsilon}$, and according to eq. 4,

$$\frac{1}{\Upsilon} \equiv \lim_{x \to \infty} e^{\frac{-f(x)\Delta n}{kT}} \qquad (12)$$

for respective models and reaction conditions. $\frac{1}{\Upsilon}$ is always less than 1 as it is the exponential of the bias energy from a downward force on the faster tube. $\left(\frac{1}{\Upsilon}\right)^{-1}$, on the other hand, equals $\lim_{x \to -\infty} e^{\frac{-f(x)\Delta n}{kT}}$ and is the *down-break* speed modifier.

The growth speed at an *up-break* boundary tube in a MWNT (from eq. 7) is,

$$K_i(t) \propto \chi_i e^{\frac{-f_{i,i-1}\Delta n}{kT}} \cdot \lim_{x \to \infty} e^{\frac{-f(x)\Delta n}{kT}} = \chi_e \qquad (13)$$

$i - 1$ tube is the jointly growing neighbor. Likewise, the growth speed of a *down-break* tube in MWNT is $K_i(t) \propto \chi_i e^{\frac{-f_{i,i-1}\Delta n}{kT}} \left(\frac{1}{\Upsilon}\right)^{-1}$. Thus the overall χ_e for these jointly growing shells can be either
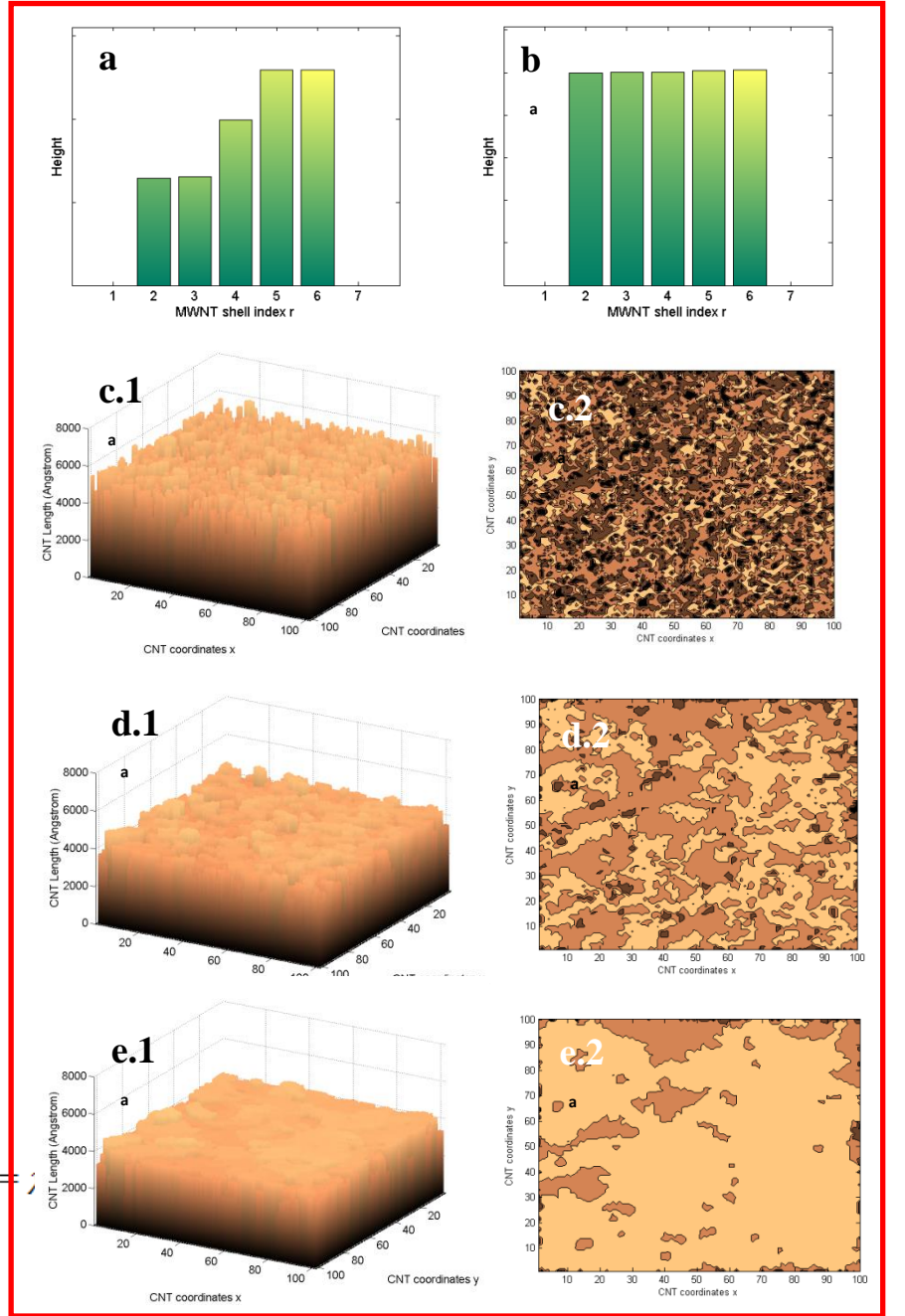

Fig. 2. simulation result. (a) and (b) are 5 shells MWNT simulations. (c), (d) and (e) are 100 by 100 CNT bundle simulation. (c.1), (d.1) and (e.1) are direct 3D plots of the simulation results. (c.2), (d.2) and (e.2) are contour plots of the same results. Simulation parameters are in Table I.

TABLE I
PARAMETERS OF SIMULATION

FIGURE	SIZE	CHIRAL ANGLE RANGE χ	DIAMETER d (nm)	PRECURSOR SIZE Δn
MWNT a	5	$1-30$	$0.5-2.5$	1
MWNT b	5	$1-30$	$3.0-5.0$	1
Bundle c	100*100	$5-20$	1.1	1
Bundle d	100*100	$5-20$	1.1	3
Bundle e	100*100	$5-20$	1.1	6

18

$\sqrt{\chi_1\chi_2\cdots\chi_N\left(\frac{1}{\gamma}\right)^2}$ if both the inner and outer boundary tubes are *up-breaks* (e.g. ambient spaces at both boundaries) or $\sqrt{\chi_1\chi_2\cdots\chi_N}$ if the inner boundary is an *up-break* and outer is a *down-break*. No other cases are possible as the inner shell is not allowed to penetrate the outer shell.

The boundary tubes of a jointly growing domain in a bundle can have a combination of joint-growth, up-breaks and down-breaks among its 6 neighbors. We generalize the equilibrium coefficient to be

$$\chi_e = \sqrt{\chi_1\chi_2\cdots\chi_N\left(\frac{1}{\gamma}\right)^m} \qquad (14)$$

where m is an integer depending on specific morphology of the domain.

Before the steady state growth is reached, tubes grow in a heat equation analogous behavior. In order to analyze the initial growth kinetics, we assume small length deviation and linearize the force curve according to the slope around x=0. This slope is denoted as α and the inter-tube spacing is $\Delta r = 3.4\text{Å}$. Using a continuous model in a MWNT, we define $l(r,t)$ as the length of the tube at r radial distance from the central axis of the MWNT at time t, and χ_r is the chiral angle of this tube. The force component equals

$$-\sum_j f_{r,j}\Delta n = -(f_{r,r-1}+f_{r,r+1})\Delta n \approx \alpha\,\frac{\partial^2 l(r,t)}{\partial r^2}\cdot\Delta n\Delta r^2 \quad (15)$$

Subsequently, using second order Taylor expansion, we find the MWNT growth partial differential equation from eq. 7.

$$\frac{\partial l(r,t)}{\partial t} = C\cdot\chi_r e^{\frac{-\sum_j f_{r,j}\Delta n}{kT}} = C\cdot\chi_r\left(\frac{\alpha}{kT}\frac{\partial^2 l(r,t)}{\partial r^2}\cdot\Delta n\Delta r^2 + 1\right) \qquad (16)$$

Here, C is a constant equals to $A\cdot e^{-\frac{E_A^\circ}{kT}}$ in eq. 7.

We use hexagonal coordinates *i,j,k* to analyze tubes in a bundle. We have $l(i,j,k,t)$ as the length of the tube at coordinate (*i, j k*) at time t. We notice that any tube in a bundle belongs to three lines of tubes along *i, j* and *k* directions. Similar analysis in MWNT is applied to CNTs in bundle on each line and yields the bundle growth partial differential equation,

$$\frac{\partial l(i,j,k,t)}{\partial t} = C\cdot\chi_{i,j,k}\left[\frac{\alpha}{kT}\left(\frac{\partial^2 l(i,j,k,t)}{\partial i^2}+\frac{\partial^2 l(i,j,k,t)}{\partial j^2}+\frac{\partial^2 l(i,j,k,t)}{\partial k^2}\right)\Delta n\Delta r^2 + 3\right] \qquad (17)$$

α is the near $x = 0$ slope of the force of tube pair (Fig. 1. d, red curve).

We performed real time simulation on different MWNT and bundle configurations.

Simulation procedure. This simulation begins by generating random chiral angles χ within an assigned range for all CNTs. For computational efficiency, our algorithm employs three straight-line segments to approximate the arctangent force curves. In each time step Δt, the algorithm finds the "$-\sum_j f_{i,j}\Delta n$ for all CNTs according to its length deviations from its neighbors and evaluates the growth rate K at time t based on eq. 7. Subsequently it updates the length of all tubes to the time $t + \Delta t$ by,

$$l(coor, t + \Delta t) = l(coor, t) + K(coor, t) \cdot \Delta t \quad (18)$$

"coor" specify the coordinates of the tube and it is the radial distance index r from the center for MWNT and 2-D indexes for bundles. Tubes in the bundle are treated as hexagonally densely packed with 6 neighbors of adjacent indexes. Zero length tubes are also added as the ambient space surrounding the MWNT or bundle.

Because we are only interested in the relative morphology features at steady state, we select an arbitrary value for the constant part $A \cdot e^{-\frac{E_A^\circ}{kT}}$ and ignored the absolute output height. Since most CVD reaction temperatures ranges from 900K to 1200K, the temperature difference only has minor influence of the growth speed ratio between tubes, which determines whether a break-off occurs. We held temperature at 973K and experimented with different precursor size Δn and MWNT diameters, as shown in Table I.

Simulation results show clear correlation between the magnitude of van der Waals interaction and the nanotube length morphology. MWNT shells at small diameters tend to break off from their neighbors because the cap effect is weak and tubes become inseparable at large cap effect. Lack of cap effect, the interaction force on tubes in a bundle does not increase with diameter. Its length adjusting effect is not obvious at similar conditions. Yet as the precursor size Δn increases, the bias energy $-\sum_j f_{i,j} \Delta n$ also increases proportionally. Simulation result in Fig 2. d and e depicts the merge of jointly growing domains as Δn increases. At $\Delta n = 3$, the contour (Fig. 2. d.2) indicates significant increase of domain size, and $\Delta n = 6$, the CNT carpet becomes visually flat.

Our research suggests that Van der Waals interaction force between nanotubes is able to substantially influence tube growth kinetics. This force establishes a local feedback mechanism that accelerates the shorter tube growth and slows down the longer tube growth. Tubes within one jointly growing domain grow at a speed proportional to a modified geometric mean of their chiral angles. Simulation shows at typical reaction condition, large diameter MWNT and large reaction precursor will greatly enhance the effect of the force.

Our mathematical abstraction may not precisely govern the behaviors of tubes that are not nucleated simultaneously or non-vertical tubes with many defects, but it provides a generalization that matches most experimental observations. Further research on this mechanism may lead to interesting mathematical solution of the complex system and may reveal new insights into force induced nanotube termination.

References to Section III

[1]   Feng, D ; Yakobson, B.I. *Dislocation theory of chirality-controlled nanotube growth*. PNAS 2009, 2506 – 2509.

[2]   Yamada T ; Namai T. ; Iijima, S. *et al. Size-selective growth of double-wall carbon nanotube forests from engineered iron catalysts*. Nnano. 2006. 95.

[3]   Ebbesen, T.W. *Carbon Nanotubes*. Annu. Rev. Mater. Sci. 1994. 24 : 235 - 64

[4]   Iijima S, Ajayan PM, Ichihashi T. *Growth model for carbon nanotubes*. Phys RevLett 1992 69:3100–3103.

[5]   Iijima, S. *Growth of carbon nanotubes*. Mat. Sci. & Engin, 1993, B19:172–180.

[6]   Thess A, et al. *Crystalline ropes of metallic nanotubes*. Science 1996, 273:483–487.

[7]   Maiti A. ;Brabec CJ ; Roland CM ; Bernholc J. *Growth energetics of carbon nanotubes*. Phys Rev Lett 1994, 73:2468–2471.

[8]   Coleman, J. N.; Khan, U.; Gun'ko, Y. K. *Mechanical reinforcement of polymers using carbon nanotubes*. Adv.Mater. 2006, 18, 689–706.

[9]   Wei, C.; Dai, L.; Roy, A.; Tolle, T. B. *Multifunctional chemical vapor sensors of aligned carbon nanotube and polymer composites*. J. Am. Chem. Soc. 2006, 128, 1412–1413.

[10]   Li, J.; Koehne, J. E.; Cassell, A. M.; Chen, H.; Ng, H. T.; Ye, Q.;Fan, W.; Han, J.; Meyyappan, M. *Inlaid multi-walled carbon nanotube nanoelectrode arrays for electroanalysis*. Electroanalysis 2005, 17, 15 – 27.

[11]   Lee, Y. H.; An, K. H.; Lee, J. Y.; Lim, S. C. *Carbon nanotubebased supercapacitors*. In Encyclopedia of Nanoscience and Nanotechnology; Nalwa, H., Ed.; American Scientific Publishers: Stevenson Ranch, CA, 2004; Vol. 1, pp 625–634.

[12] Yildirim, T.; Ciraci, S. *Titanium-decorated carbon nanotubes as a potential high-capacity hydrogen storage medium.* Phys. Rev. Lett. 2005, 94, 175501.

[13] Kreupl, F.; Graham, A. P.; Duesberg, G. S.; Steinhögl, W.; Liebau, M.; Unger, E.; Hönlein, W. *Carbon nanotubes in interconnect applications.* Microelectron. Eng. 2002, 64, 399–408.

[14] Li, S.; Yu, Z.; Rutherglen, C.; Burke, P. J. *Electrical properties of 0.4 cm long single-walled carbon nanotubes.* Nano Lett. 2004, 4, 2003–2007.

[15] Hong, B. H.; Lee, J. Y.; Beetz, T.; Zhu, Y.; Kim, P.; Kim, K. S. *Quasi-continuous growth of ultralong carbon nanotube arrays.* J. Am. Chem. Soc. 2005, 127, 15336–15337.

[16] Girifalco, L. A. ; Hodak, M ; Lee, R. S. *Carbon nanotubes, buckyballs, ropes, and a universal graphitic potential.* PRB, 2000. 0163 - 1829

[17] Girifalco, L.A. ; Lad, R.A. *Molecular Properties of fullerene in the gas and solid phases.* J. Phys. Chem., 1992. 858 – 861

[18] **Tersoff, J. ; Ruoff, R.S. Structural Properties of a Carbon-Nanotube Crystal. Phys. Rev. Lett. 1994, 73, 676–679**

[19] Yu, M.F. ; Yakobson, B.I. ;Ruoff, R.S. *Controlled Sliding and Pullout of Nested Shells in Individual Multiwalled Carbon Nanotubes.* J. Phys. Chem. B 2000, 104, 8764-8767

[20] Clauss, W.; Bergeron, D.J.; Johnson, A. T. *Atomic resolution STM imaging of a twisted single-wall carbon nanotube.* Phys. Rev. B, 1998, 58, R4266 – R4269.